Supplemental document accompanying submission to *Optica*

Title: Spatiotemporal refraction of light in an epsilon-near-zero ITO layer

Authors: Justus Bohn, Ting S. Willie Luk, S. A. R. Horsley, Euan Hendry

Submitted: 7/9/2021 6:07:21 AM

Supplement 1: Spatiotemporal refraction of light in an epsilon-near-zero ITO layer: frequency shifting effects arising from interfaces

CONTENTS

S1 Methods 2
- A ITO sample fabrication . . . 2
- B Experimental set-up . . . 2

S2 Thin layer model 3

S3 Thickness dependent refractive index 4

S4 Calculation of transmitted pulse spectrum 6

S5 Additional measurements 7
- A Wavelength dependence . . . 7
- B Intensity dependence . . . 8
- C Blueshifted spectrum . . . 9

S1. METHODS

A. ITO sample fabrication

We utilise ITO samples of different thicknesses. For the 107 nm sample, the ITO was sputtered onto a coverslip at room temperature using 90/10 In_2O_3/SnO_2 Kurt Lesker target and sputtering tool. The base pressure before the deposition was in low 10^{-6} torr but raised to 3 mT of Ar only during deposition with an RF power of 145 W. In order to achieve high carrier density, both deposition and annealing were performed in the lowest possible residual oxygen environment. The samples are post-annealed in forming gas for 3 min at temperatures between 425-525°C in a rapid thermal annealer. The 407 nm sample was obtained from UQG Ltd.

The optical properties and thicknesses of the indium tin oxide (ITO) samples are characterised using an ellipsometer. The ellipsometry data was using Tauc-Lorentz and Drude models. The extracted optical parameters are listed in Table S1, where the epsilon-near-zero (ENZ) frequency is calculated as $f_{ENZ} = \frac{1}{2\pi}\sqrt{\omega_p^2/\varepsilon_\infty - \gamma^2}$. The corresponding wavelength-dependent permittivity and refractive index are plotted in Figure S1.

Table S1. Drude parameters for the different ITO film thicknesses.

t_{ITO} (nm)	ε_∞	$\omega_p(10^{15}$ rad/s)	ω_p/γ	f_{ENZ} (THz)
407	3.45	2.5	11.5	212
115	3.81	3.03	16.9	246

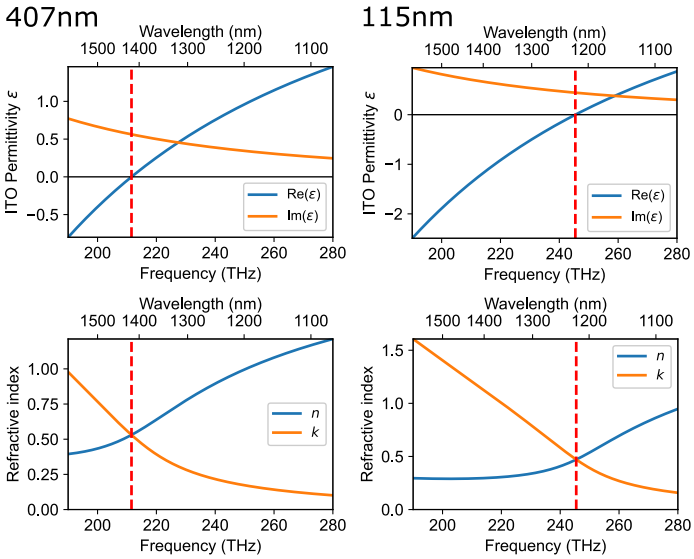

Fig. S1. Optical properties of indium thin films. Optical permittivity (top) and refractive index (bottom) are plotted for the two different samples. The ENZ frequency is marked at 212 THz for the 407 nm sample (left), 246 THz for 115 nm (right).

B. Experimental set-up

For the pump-probe measurements, we used an amplified Ti:sapphire laser (Legend Elite, Coherent), with a central wavelength of 800 nm, pulse duration of 107 fs and repetition rate of 1 kHz, feeding two identical OPAs (TOPAS, Light Conversion). The signal output of one OPA was used as the pump, and the signal output of the other OPA was used as the probe, allowing us independent control of pump and probe frequencies. The pump was focused using a 30 cm BK7 lens, the probe with a 25 cm $CaFl_2$ lens. The pump beam diameter (1/e) was measured to be 480 µm in air, while the probe was 250 µm. To make sure the incident intensity of the probe is significantly smaller than the pump, we used several additional OD filters to decrease the probe

power and tested that the nonlinear reflection was independent of adding/removing filters. The angle of incidence of the pump is 5° smaller than that of the probe. For the spectral analysis, we used an Andor Shamrock 163 spectrograph with a DU490A-1.7 camera.

S2. THIN LAYER MODEL

The thin layer model is based on the transfer matrix method (TMM), which simplifies to the Airy formula for the three-layer case (1. air, 2. ITO, 3. substrate):

$$t_{13} = \overbrace{\frac{1}{1 + r_{12} r_{23} e^{2ik_2 d}}}^{\text{internal reflections}} \underbrace{t_{12} t_{23}}_{\text{interface transmission}} \overbrace{e^{ik_2 d}}^{\text{bulk propagation}} . \tag{S1}$$

The transmission coefficient (t_{13}) of the layer can be calculated using the ITO thickness (d), the in-plane wavevector component inside the ITO layer ($k_2 = n_{\mathrm{ITO}} k_0 \cos\theta_2$) and the Fresnel coefficients of the front (r_{12}, t_{12}) and back interface (r_{23}, t_{23}). Here, the $e^{ik_2 d}$-term describes the bulk propagation term, and time-dependent phase changes of it have been discussed as temporal refraction. Considering the multiplication of complex numbers leads to the addition of phases it follows:

$$\Delta\Phi_{13} = \overbrace{\Delta\Phi_{\mathrm{ir}} + \Delta\Phi_{12} + \Delta\Phi_{23}}^{\text{interface effects}} + \overbrace{\Delta\Phi_{\mathrm{b}}}^{\text{bulk propagation}} . \tag{S2}$$

The interface contributions appear from the Frensel transmission coefficients (Φ_{12}, Φ_{23}) and the internal reflections term $\Phi_{\mathrm{ir}} = \arg(1/(1 + r_{12} r_{23} e^{2ik_2 d}))$. Moreover, the expected frequency shifts are:

$$\Delta f_{13} = \overbrace{\Delta f_{\mathrm{ir}} + \Delta f_{12} + \Delta f_{23}}^{\text{spatiotemporal refraction}} + \overbrace{\Delta f_{\mathrm{b}}}^{\text{temporal refraction}} . \tag{S3}$$

This paper investigates the case where the temporal refraction is no longer large compared to the frequency shift contributions induced by the spatial boundary. To simulate the temporal changes to the transmission amplitude and phase, we introduce a time-varying bulk plasmon frequency of up to 10 % reduction. The temporal shape is given by a convolution of a Gaussian with a full-width-half-maximum pulse length of 107 fs and a 300 fs exponential decay (see Figure S2a) and corresponds to the example plotted in **Figure 2** of the manuscript. Additionally, we plot the time-dependent permittivity, highlighting the ENZ crossing. The temporal changes of the phase plotted in **Figure 2b** result in frequency shifts that are shown in Figure S2b.

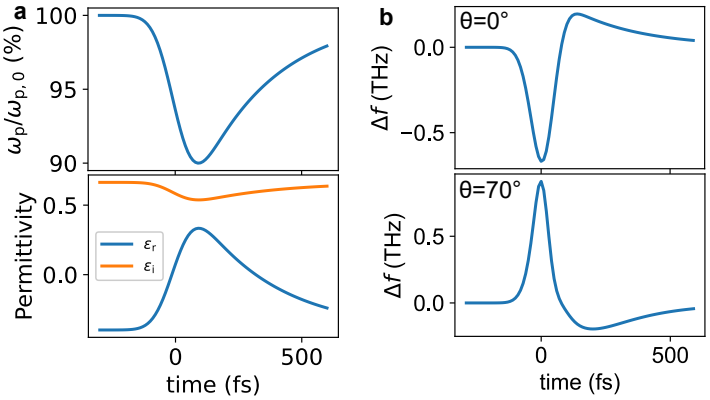

Fig. S2. Spatiotemporal refraction: frequency shifts (corresponding to Figure 2). We study the impact of a typical ω_p reduction by 10 %, as plotted **a**. The resulting permittivity is plotted for the case of the 407 nm ITO sample parameters at 200 THz. The ENZ case is passed at roughly the maximum slope. **b**, The expected frequency shifts for the transmitted probe are calculated using Δf_{13} and plotted for the normal and high angle incidence case.

The origin of these phase shifts can best be dissected by investigating the constituents of the transmittance coefficient Equation S1. We compare in **Figure 2b** the total calculated transmission phase Φ_{13} with the Fresnel transmittance coefficient phase of both interfaces (Φ_{12}, Φ_{23}) and the bulk term ($\Phi_b = \arg(e^{ik_2 d}) = nk_0 d$). In the normal incidence case, the two interface effects cancel each other out. However, the bulk contribution disappears for the high angle case, and the front interface flips the sign while the back interface remains almost unaffected. An overall transmittance phase is now decreasing instead of increasing.

Thickness dependence

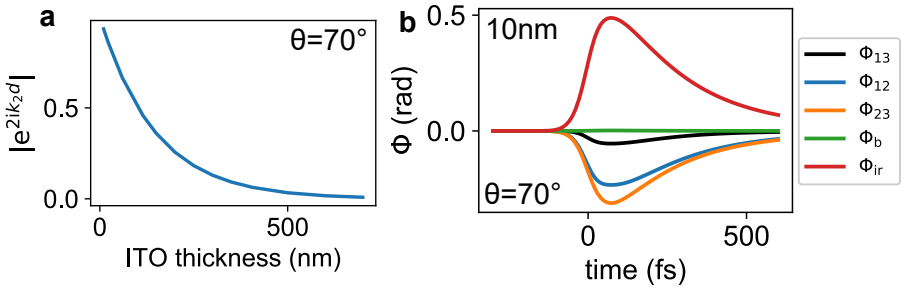

Fig. S3. Thickness dependent phase components (corresponding to Figure 4). a, We plot the absolute value of the internal reflection transmission coefficient term, showing that it only becomes comparable to 1, and therefore relevant, for $d \lesssim 200\,\text{nm}$. **b**, For the very thin case of 10 nm ($e^{2ik_2 d} \sim 1$) the internal reflection based phase shifts becomes large and compensates transmission-based effects.

Going to small thicknesses ($d \ll 1/2\,\text{Im}(k_2)$), the multiple internal reflection based denominator becomes relevant (see Figure S3a), and the phase shift of the internal reflection compensate the transmission based effects (see Figure S3b). Hence, the blueshift is expected to decreases for thicknesses smaller than $\sim 200\,\text{nm}$ as seen in **Figure 4**a of the manuscript.

Frequency dependence

To study the frequency shifting behaviour over large frequency and angle ranges, we exclusively investigate the maximum frequency shift (see Figure S4). For both the 407 nm and 115 nm sample, the blueshifted feature appears only for a large angle of incidence, as established earlier. Additionally, this blueshift occurs only for frequencies just below the (initial) ENZ case. The region of maximum blueshift sits right between the initial and pumped ENZ frequency case. This can be understood by considering the Fresnel coefficient of the front interface, which dominantly affects this feature plotted in **Figure 2b**. For the ENZ case Taylor expansion slightly below 90° the coefficient is given as ($\theta \lessapprox \pi/2, \theta_2 \ll \theta \to n_{\text{ITO}} \ll 1$, TM-polarization):

$$t_{12}(\tau) \propto \sqrt{\frac{\varepsilon_{\text{ITO}}(\tau)}{\varepsilon_{\text{ITO}}(\tau) - 1}} \overset{|\varepsilon_{\text{ITO}}| \ll 1}{\approx} i\sqrt{\varepsilon_{\text{ITO}}(\tau)}, \tag{S4}$$

with τ being the time delay between pump and probe pulse. One can see, t_{12} reduces in phase upon crossing the ENZ case (starting from negative ε_r values as seen in Figure S2a).

S3. THICKNESS DEPENDENT REFRACTIVE INDEX

To test the model, we put the implicit assumption under test that the transmission changes and phase changes have the same origin, a redshift in ω_p. The transmission changes are linked to the redshifting of ω_p. These can be used to calculate all-optical parameter changes of interest. In **Figure 5a** and Figure S5a, we show the case of using a uniform ITO layer excitation and find that the blueshift seems to be a bit overestimated. For a first improvement, we assume a spatial dependence of the ω_p in ITO. This results in a graded refractive index (GRIN) profile. We use the transfer matrix method to calculate the depth-dependent absorption of the pump inside the ITO layer as seen in Figure S5b and scale the distribution. The front will be most affected by pumping, and t_{12} driven effects may saturate sooner, while the overall blueshift may be smaller as the angle independent t_{23} contribution (see Figure S3a) becomes smaller. This can be seen in **Figure**

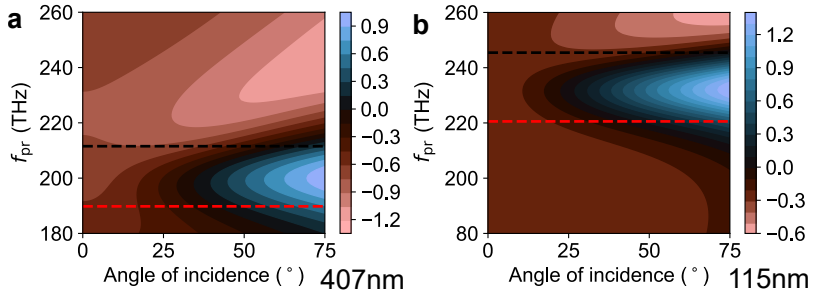

Fig. S4. Angle and frequency dependent spatiotemporal refraction behaviour. We plot the frequency shifts as seen in Figure S2b for the maximum case of $\tau = 0$ fs and study the probe frequency and angle dependence for the case of the 407 nm (**a**) and the 115 nm (**b**) parameters. The black dashed line indicates the initial f_{ENZ}, while the red dashed line indicates the pumped case.

5a or Figure S5c of our thickness dependent model application, which behaves qualitatively very similar to the uniform layer plotted in a, but has a significantly smaller blueshift. This also corresponds better to what is measured in experiment. While this depth-dependent plasma frequency should still be seen as a rough assumption, it appears to be noticeably more accurate than simply taking a uniform layer.

We also present the extracted ω_p values averaged over the layer thickness are plotted in Figure S5d. The modulation of up to ~10 % are in good agreement with similar studies [1]. Also, the increased angle leads to a reduced incident intensity due to a stretched out elliptical beam-sample cross-section area. Hence, a more minor bulk plasma modulation is seen for higher angles.

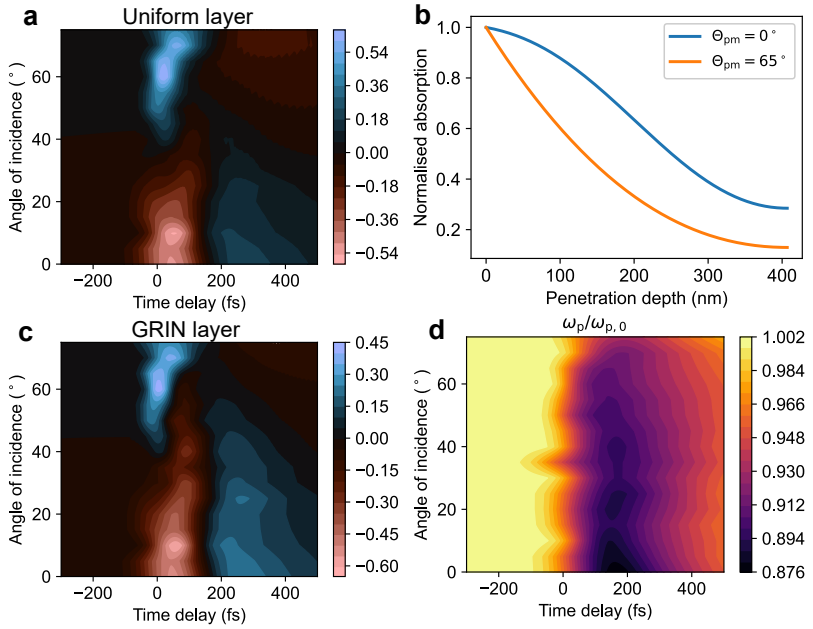

Fig. S5. Uniform vs GRIN layer (corresponding to Figure 5). a, The plotted frequency shift estimates are based on the time-dependent transmission phase, calculated via the uniform layer assumption ($I_0 = 400\,\mathrm{GW\,cm^{-2}}$,$f_{pm} = 250$ THz, $f_{pr} = 200$ THz, TM analyser). **b**, The normalised depth-dependent absorption of the TE polarised pump for the low and high angle case plotted in **Figure 3b**. **c**, The GRIN based frequency shift estimates, utilising the depth-dependent plasma frequency. **d**, The plasma frequencies plotted correspond to the transmission changes measured in the experiment **Figure 4b**.

S4. CALCULATION OF TRANSMITTED PULSE SPECTRUM

It is difficult to solve Maxwell's equations in a time-dependent dispersive medium, even a homogeneous one. To obtain an approximate form of the transmitted pulse in our system we reinterpret our incident pulse $H_\mathrm{i}(t)$ as a sum of delta function pulses each of amplitude $H_\mathrm{i}(\tau)$, arriving at time τ, i.e.

$$H_\mathrm{i}(t) = \int_{-\infty}^{\infty} d\tau \delta(t-\tau) H_\mathrm{i}(\tau). \tag{S5}$$

the spectral decomposition of which is

$$\tilde{H}_\mathrm{i}(\omega) = \int_{-\infty}^{\infty} d\tau \mathrm{e}^{\mathrm{i}\omega\tau} H_\mathrm{i}(\tau) \tag{S6}$$

While the delta pulse of amplitude $H_\mathrm{i}(\tau)$ propagates through the structure, the frequency-dependent transmission coefficient is taken to have the approximately constant value $t(\tau,\omega)$. This assumes that the permittivity remains approximately constant during the ring-down time of the structure. Using (S6), the spectrum of the transmitted pulse can then be written as

$$\tilde{H}_\mathrm{t}(\omega) = \int_{-\infty}^{\infty} d\tau\, t(\tau,\omega)\, \mathrm{e}^{\mathrm{i}\omega\tau} H_\mathrm{i}(\tau). \tag{S7}$$

Using the inverse Fourier transform of Eq. (S6) we can then rewrite the transmitted spectrum (S6) in terms of the incident one, rather than the incident amplitude $H(\tau)$

$$\tilde{H}_\mathrm{t}(\omega) = \int_{-\infty}^{\infty} \frac{d\omega'}{2\pi}\, t(\omega-\omega',\omega)\, \tilde{H}_\mathrm{i}(\omega'), \tag{S8}$$

where

$$t(\omega-\omega',\omega) = \int_{-\infty}^{\infty} t(\tau,\omega) \mathrm{e}^{\mathrm{i}(\omega-\omega')\tau} \tag{S9}$$

We numerically implemented (S8) to calculate the transmitted spectra of our pulses, using a Fast Fourier transform to calculate $t(\omega-\omega',\omega)$, then treating the convolution (S7) discretely as a matrix multiplication, for a fixed frequency resolution $\Delta\omega$.

S5. ADDITIONAL MEASUREMENTS

Here, we present further experimental data to support the previously discussed scenarios.

A. Wavelength dependence

The ENZ wavelength of the 407 nm sample is 1417 nm. We show in Figure S6 that the blueshift does not appear above the ENZ case. Additionally, we show that it is reserved for TM polarisation.

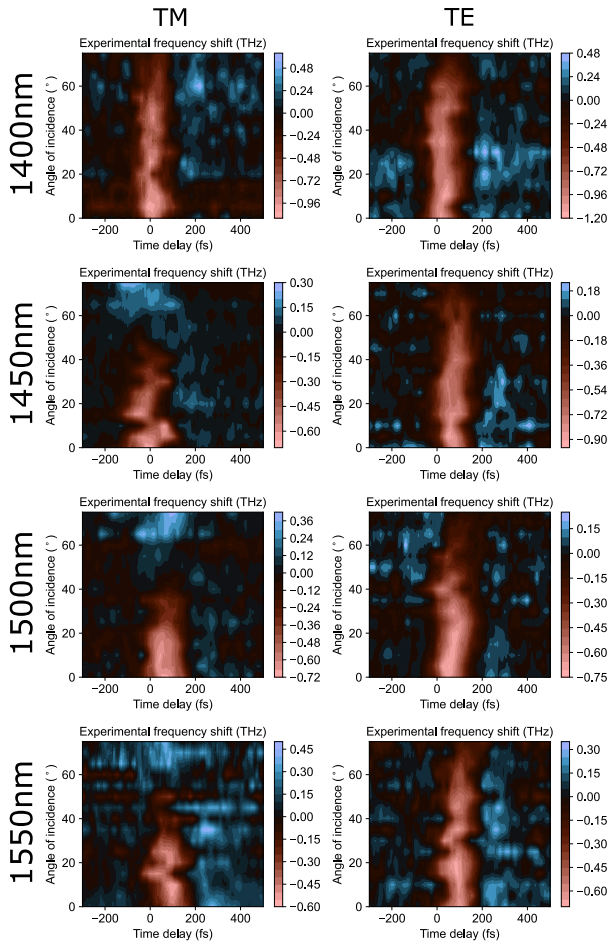

Fig. S6. Wavelength and polarisation dependence. The measured frequency shifts show the wavelength dependence. Additionally, the TE case is measured by rotating the analyser. ($I_0 = 400\,\mathrm{GW\,cm^{-2}}$, $f_{\mathrm{pm}} = 250\,\mathrm{THz}$).

B. Intensity dependence

The intensity-dependent measurements are done for 100 to 400 GW cm^{-}2 for both samples and plotted in Figure S7. The redshift feature appears to saturate slightly faster for the 115 nm sample than for the 407 nm. The blueshift feature appears to start saturating for both samples roughly at 200 GW cm^{-}2 incident intensity.

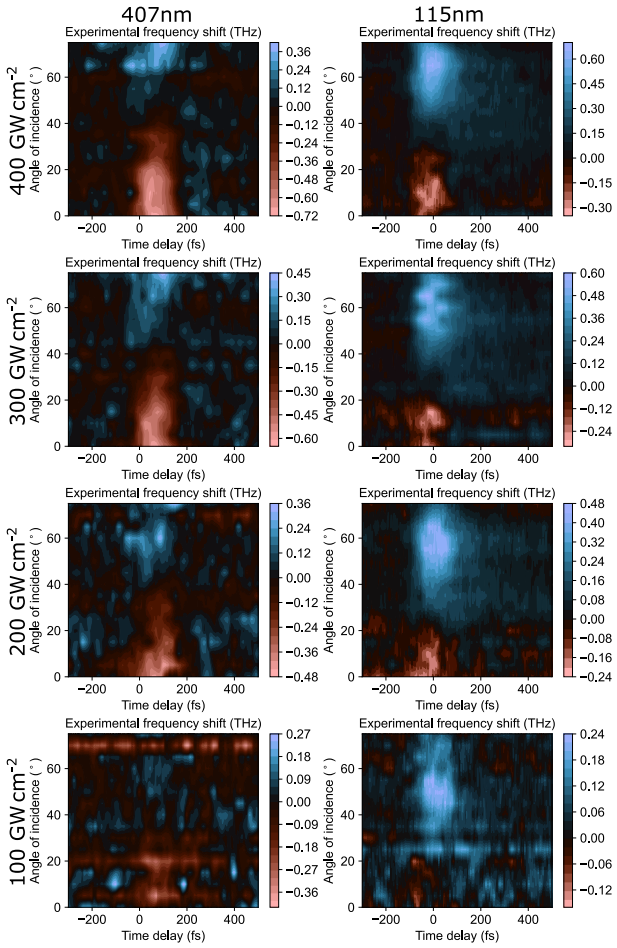

Fig. S7. Intensity dependence. The measured frequency shifts show the incident intensity dependence of the TM contribution. This was done for both samples: 407 nm ($f_{\mathrm{pm}} = 250$ THz, $f_{\mathrm{pr}} = 200$ THz) and 115 nm ($f_{\mathrm{pm}} = 214$ THz, $f_{\mathrm{pr}} = 240$ THz).

C. Blueshifted spectrum

We present the example of the strongest measured blueshift feature, given by the 115 nm film as seen in Figure S8 and shown in **Figure 5a** of the manuscript.

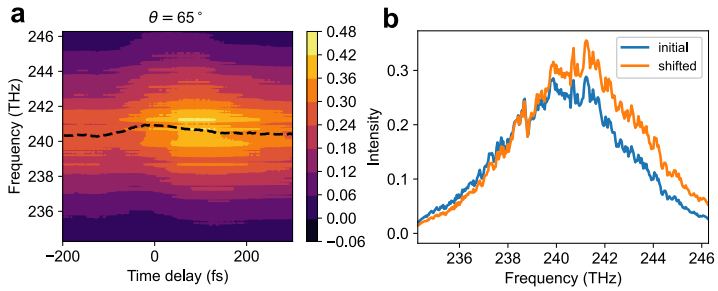

Fig. S8. Blueshifted spectrum (corresponding to Figure 4c). a, For the 115 nm sample, the time-dependent spectrum was measured. The incident pump intensity is 400 GW cm^{-}2. The dashed line indicates the traced central frequency position. **b**, The pump free initial spectrum (blue) is plotted along with the maximum shifted case (orange).

REFERENCES

1. J. Bohn, T. S. Luk, C. Tollerton, S. W. Hutchings, I. Brener, S. Horsley, W. L. Barnes, and E. Hendry, "All-optical switching of an epsilon-near-zero plasmon resonance in indium tin oxide," Nat. Commun. **12**, 1017 (2021).